Received: 22 July 2019 | Revised: 4 October 2019 | Accepted: 10 October 2019

DOI: 10.1002/qua.26092



REVIEW

International Journal of QUANTUM CHEMISTRY WILEY

# External electric field effect on electronic properties and charge transfer in $CoI_2/NiI_2$ spinterface

Iuliia Melchakova[1,2,3] | Evgenia A. Kovaleva[1,2] | Natalia S. Mikhaleva[1] | Felix N. Tomilin[1,2] | Sergey G. Ovchinnikov[1,2] | Alexander A. Kuzubov[†] | Paul Avramov[3]

[1]Siberian Federal University, Krasnoyarsk, Russia

[2]Kirensky Institute of Physics, Krasnoyarsk, Russia

[3]Department of Chemistry, Kyungpook National University, Daegu, South Korea

**Correspondence**
Iuliia Melchakova, Department of Chemistry, Kyungpook National University, 80 Daehak-ro, Buk-gu, Daegu (41566), Korea.
Email: iuliia.melchakova@gmail.com

**Funding information**
Ministry of Education and Science of the Russian Federation, Grant/Award Number: 16.1455.2017/PCh; National Research Foundation of Korea, Grant/Award Number: NRF-2017R1A2B4004440; Russian Foundation for Basic Research, Government of Krasnoyarsk Territory, Krasnoyarsk Regional Fund of Science, Grant/Award Number: 18-43-243011

## Abstract

Electronic structure and spin-related properties of $CoI_2/NiI_2$ heterostructure were studied by means of density functional theory. It was shown that the electronic structure at the Fermi level can be characterized by a band gap. The effect of the external electric field on charge transfer and electronic properties of the $CoI_2/NiI_2$ interface was investigated, and it was found that band gap width depends on the strength of the applied electric field, switching its nature from semiconducting to a half-metallic one. An easy control of the electronic properties and promising spin-polarized nature of the $CoI_2/NiI_2$ spinterface allows the heterostructure to be used in spin-related applications.

**KEYWORDS**

DFT, electric field, Hubbard correction, spintronics, transition metal dihalides

## 1 | INTRODUCTION

An important breakthrough in materials science in recent years is primarily associated with the synthesis of novel two-dimensional materials.[1–3] The pioneer in such materials is graphene through a graphite low-dimensional structural analog. The absence of intrinsic spin polarization in graphene limits its applications as a spacer in various layered heterostructures.[4,5] The heterostructures draw great attention due to unique properties that can find an application in new branches of fundamental science (eg, spintronics). Spintronics required special properties in materials that separate different spin ordering. One of these properties is a half-metallic conductivity. The half-metallic compounds have more benefits in use due to the nonzero density of states at the Fermi level for one spin channel and semiconducting band gap for another one.

Transition metal dichalcogenides (TMDs)[6,7]—a family of layered compounds with adjacent layers bonded by weak van der Waals forces—are considered promising materials for spin-related applications due to the wide variety of conducting properties (from metallic to semiconducting) with direct or indirect band gaps. However, their applications are limited due to the absence of net magnetic moments for most of TMDs, except of $VS_2$ and $VSe_2$.[8–11] From this point of view, transition metal dihalides[12,13] (TMH2), being structurally analogous to TMD, are remarkable candidates for spin-related applications. Unlike TMDs, most of the TMH2 have nonzero magnetic moments on TM ions that create a great opportunity to vary properties using magnetic fields and other magnetic phenomena.

Bulk $CoI_2$ and $NiI_2$ are A-type antiferromagnets with spins aligned along with the metal-iodine bonds, which is confirmed by Mossbauer spectroscopy measurements.[14] Cobalt iodide possesses CdI2-type 1T structure (P-3m1 space group), while $NiI_2$ obeys the $CdCl_2$-type structure (R-3m:H space group) with ABC stacking of nickel and iodine ions. There are two possible configurations of $TMH_2$ monolayers, namely, H (trigonal prismatic) and T (octahedral), which differ from each other by the orientation of second-layer ligand atoms with respect to the first-layer ligands.[8]

[†]Deceased December 31, 2016

  

Numerous studies demonstrated that magnetic and spin properties of low-dimensional nanomaterials fundamentally differ from those of the bulk due to an atom magnetic moment's strong dependence on its coordination number. For example, the study of electronic and magnetic properties of CrN monolayer performed by Zhang[15] showed that, unlike the bulk antiferromagnetic phase, its 2D counterpart is ferromagnetic half-metal, thermally and mechanically stable. Hexagonal configuration of the CrN monolayer, which may be obtained by using substrates such as $MoS_2$ and $MoSe_2$ with suitable structural parameters, was predicted to possess half-metallic properties as well.[16]

The previously mentioned trend is also fair to $CoI_2$ and $NiI_2$ structures. It was estimated that atomic coordination in $CoI_2$ and $NiI_2$ monolayers are similar to correspondent octahedral 3D analogs.[17] It was found that the single-layer $TMH_2$ retains the semiconducting type of the band gaps, but in contrast to bulk, spin alignment could be characterized as ferromagnetic (parallel to z-direction).[12] It was also found that lattice parameters of $CoI_2$ and NiI monolayers in T-configurations have good coincidence (lattice difference ~0.25%), which implies the absence of moire pattern and distortion of the initial structure.

The point of this article is to design a new semiconducting heterostructure with interesting spin-related properties at PBE/GGA level of theory with a tunable band gap via the external impact.

## 2 | METHODS

All electronic structure calculations of individual TM$Hal_2$ fragments and $CoI_2/NiI_2$ spinterfaces were performed within the framework of density functional theory (DFT) using PBE exchange-correlation functional[18,19] and pseudoatomic orbitals with norm-conserving Vanderbilt pseudopotentials,[20] as implemented in the open-source package OpenMX.[21] In order to account for the correlation effects, which are usually significant in transition metal compounds, the simplified form of the Hubbard U correction proposed by Dudarev et al.[22,23] was implemented. The effective $U$ parameters ($U_{eff} = U - J$; $U$ stands for the Coulomb repulsion, and $J$ is the exchange parameter) for TM atoms were 3.3 and 4.6 eV for cobalt and nickel atoms, respectively.

The $CoI_2/NiI_2$ spinterface was designed by stacking of $NiI_2$ and $CoI_2$ T-monolayers one above the other at a distance of 3.72 Å (Figure 1) that were cut out along (001) the direction of the bulk crystals (Figure S1). The unit cell optimizations were performed until the maximum force acting on atoms was less than 0.001 eV/Å. The Mönkhorst-Pack[24] scheme was implemented for $k$-point Brillouin zone sampling with $k$-point grid-contained $9 \times 9 \times 1$ points. A vacuum interval of 20 Å was set to normal in the monolayer plane in order to prevent artificial interactions in periodic boundary conditions.

To study the halide bulk crystal spin properties, several different types of spin ordering were considered. The energy difference between the ferromagnetic and antiferromagnetic states per formula unit in $NiI_2/NiI_2$ and $CoI_2/CoI_2$ bilayer structures with two TM ions (Figure S2, Table 1) was calculated as:

$$\Delta E = E_{fer} - E_{afer}, \tag{1}$$

where $E_{fer}$ and $E_{afer}$ are total energies of ferromagnetic and antiferromagnetic states of TM$Hal_2$-based heterostructures. For the spinterface, the energy differences were determined as:

$$\Delta E = E_{fer} - E_{ferri}, \tag{2}$$

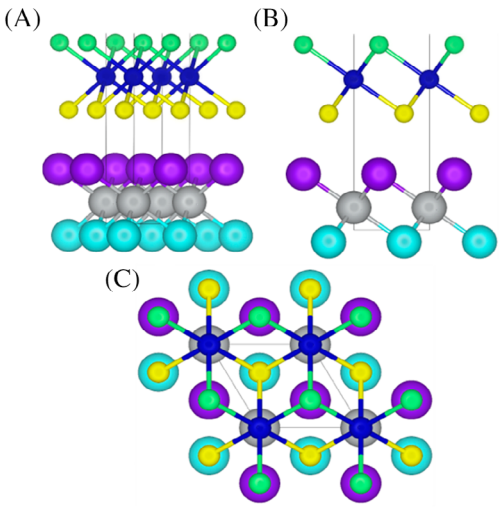


**FIGURE 1** $CoI_2/NiI_2$ heterostructure (A and B are side views; C is top view). Co and Ni ions are denoted as dark blue and gray balls, respectively. Depending on the position of the iodine ions, they are denoted as light blue ($I_1$, $NiI_2$ outer I ions), purple ($I_2$, $NiI_2$ inner I ions), yellow ($I_3$, $CoI_2$ inner I ions), and green ($I_4$, $CoI_2$ outer I ions)

**TABLE 1** Energies of $TMI_2$ structures in different magnetic states

| Hetero structure | Inter layer dist | $\Delta E$ (eV) | State | $E_{stack}$ (eV) | $\mu$ ($\mu_B$) |
|---|---|---|---|---|---|
| $CoI_2/CoI_2$ | 3.47 | −0.05 | Ferromagnetic | — | 6.00 |
| | | | Antiferromagnetic | — | 0.00 |
| $NiI_2/NiI_2$ | 3.57 | 0.01 | Ferromagnetic | — | 4.00 |
| | | | Antiferromagnetic | — | 0.00 |
| $CoI_2/NiI_2$ | 3.46 | 0.04 | Ferromagnetic | −0.12 | 5.00 |
| | | | Ferrimagnetic | −0.07 | 1.00 |

where $E_{fer}$ and $E_{ferri}$ stand for the total energies of the spinterface in ferromagnetic and ferrimagnetic states, respectively.

Stacking energies $E_{stack}$ between $CoI_2$ and $NiI_2$ monolayers per formula unit were calculated as:

$$E_{stack} = E_{spint} - E_{CoI2} - E_{NiI2}, \quad (3)$$

where $E_{spint}$ is the total energy of the spinterface, and $E_{CoI2}$ and $E_{NiI2}$ are the total energies of $CoI_2$ and $NiI_2$ free-standing fragments, respectively (Table 1).

According to the results of stacking energy calculations, the ferromagnetic state is favorable for a $CoI_2$ bilayer (contrary to bulk $CoI_2$), whereas antiferromagnetic spin ordering is favorable in the case of $NiI_2$ bilayer and $CoI_2/NiI_2$ spinterface. It was previously shown[6] that a 2D structure may actually have ferromagnetic ordering due to the confinement effect even though 3D analog possesses antiferromagnetic alignment. Close stacking energy values of ferro- and ferrimagnetic heterostructure make the creation of heterostructures with different magnetic ordering possible. Taking into account the stacking energy values (−0.12 and −0.07 eV for ferro- and ferrimagnetic states, respectively, Table 1), the ionic character of the system, and the distance between fragments, it could be assumed that the bonding of the fragments in heterostructure is primarily caused by van der Waals (vdW interactions have the energy more than 0.01 eV/atom) and exchange interactions.

In order to verify the bending structural stability of the heterostructures,[25,26] an additional calculation was performed for $NiI_2/CoI_2$ cluster. A supercell consisting of $3 \times 3 \times 1$ unit cells was chosen to design the cluster with neighboring images distinguished from each other by 10 Å of vacuum interval in each direction in order to prevent artificial interactions in periodic boundary conditions. The structural optimization was performed until the maximum force acting on atoms was less than 0.001 eV/Å. As a result, the final cluster structure was not distorted, so it proves the bending stability of the spinterface.

## 3 | RESULTS AND DISCUSSIONS

### 3.1 | Atomic structure and electronic properties of $CoI_2/NiI_2$ spinterface

Because of the same symmetry and type of the conformers, the $CoI_2/NiI_2$ spinterface was designed by stacking the $CoI_2$ and $NiI_2$ layers one above the other (Figure 1), with both TM and iodine ions placed pairwise directly above each other ($I_3$ above $I_1$, $I_4$ above $I_2$). In order to exclude the extra repulsion of iodine ions from different fragments, the $CoI_2$ monolayer was placed atop the $NiI_2$, keeping the metal ions in the same position (Co above the Ni).

The total (TDOS) and partial (PDOS) densities of states of ferromagnetic and ferrimagnetic states of $CoI_2/NiI_2$ spinterface are presented in Figure 2. In Figure 2, the TDOSs of the spinterface are indicated in black lines, and the red and blue lines represent the PDOSs of the $NiI_2$ and $CoI_2$ fragments, respectively. The TDOSs of free-standing $CoI_2$ and $NiI_2$ 2D monolayers, together with PDOSs of the $NiI_2$ and $CoI_2$ fragments in the spinterface (Figure S3a–b and c–d, respectively), are shown to analyze the nature of interlayer interactions between $CoI_2$ and $NiI_2$ fragments.

As can be seen in Figure 2, the $CoI_2/NiI_2$ spinterface is a spin-polarized narrow band gap semiconductor with a band gap of 0.84 eV at the Fermi level for ferrimagnetic ordering. The $NiI_2$ electronic subsystem makes the main contribution to the conductivity band (CB) in the energy interval from 0.4 to 0.6 eV in ferromagnetic state (Figure 2 left), while $CoI_2$ contribution dominates at 0.6 to 0.8 eV region.

It is clearly seen that the TDOS for ferrimagnetic state in the valence band (VB) region is determined by superposition of almost equal contributions of both $NiI_2$ and $CoI_2$ electronic subsystems. The DOSs in both CBs and VBs demonstrate distinctive nonequivalent and asymmetrical shapes with different populations of spin-up and spin-down states. The asymmetrical population of α- and β-spins should lead to spin polarization of the spinterface.

The comparison of the DOSs (Figure S3) clearly demonstrates significant DOS redistribution caused by the interactions between the electronic subsystems of $CoI_2$ and $NiI_2$ fragments. The fragments demonstrate semiconducting properties with zero DOSs at the Fermi level. Interactions between the fragments lead to redistribution of electronic density at both lower and higher energy peaks. The disappearance of the peak associated with $d_{z^2}$ orbitals of Co in PDOS of $CoI_2$ fragment can be caused by the change of the symmetry and Δ parameter of the ligand field of

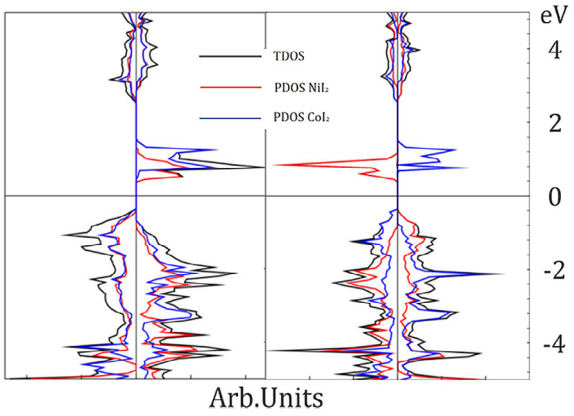


**FIGURE 2** Total and partial density of states of the $CoI_2/NiI_2$ spinterface with ferromagnetic (left) and ferrimagnetic (right) spin ordering. Black lines correspond to total densities of states (TDOSs), and red and blue lines correspond to partial densities of states (PDOSs) of $NiI_2$ and $CoI_2$ monolayers. The positive and negative intensities reflect the electronic densities of the spin-up and spin-down states

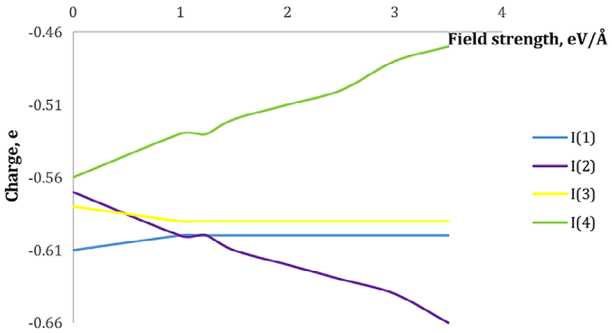


**FIGURE 3** Ionic charge dependence on the field strength for spinterface with ferromagnetic ordering. Light blue line corresponds to $I_1$ ionic charge, purple line corresponds to $I_2$ charge, yellow line corresponds to $I_3$ charge, and green line corresponds to $I_4$ charge

the Co ion in the spinterface. Exchange interactions between the fragments may also influence the PDOS shapes and occupancy numbers as the length of the vdW bonds between the $CoI_2$ and $NiI_2$ fragments (3.4 Å) is significantly shorter than the effective distances (up to 10 Å) of exchange interactions.[27]

## 3.2 | The influence of external electric field on the electronic structure of the interfaces

A set of single-point electronic structure calculations of the spinterface with external electric field strength varied from 0 to 3.5 eV/Å was performed. The ferrimagnetic spin ordering is the ground state of spinterface at low values of the electric field (lower 1.15 eV/Å). As the field strength becomes higher than 1.15 eV/Å, the ferromagnetic spin ordering becomes energetically stable.

The calculated ionic charges and magnetic moment dependences on the values of electric field strength are presented in Table S1 and Figure 3. Indexes of iodine atoms correspond to their position according to metal atoms: $I_1$ (light blue balls in Figure 1) and $I_2$ (purple balls in Figure 1) ions are located under and above Ni ions, respectively. The same notations are used for $I_3$ (yellow balls in Figure 1) and $I_4$ (green balls in Figure 1) ions for the $CoI_2$ fragment.

Increasing the external electric field strength (Figure 3) leads to the charge transfer to the $I_2$ ion of the $NiI_2$ fragment from the $I_4$ ion of the $CoI_2$ fragment. The tendency of charge transfer dependence is rather smooth for $I_1$ and $I_3$. The same tendency is fair to the spinterface with ferromagnetic ordering as well. The absolute values of TM*Hal*$_2$ fragment total net charges in both ferromagnetic and ferrimagnetic states gradually increased (See Table S1) with the increase of the electric field. To sum up, the increase of the electric field strength makes the charge localized at $NiI_2$ fragment more negative and the $CoI_2$ charge more positive.

The dependence of magnetic moments located at $CoI_2$ fragment on the electric field strength is presented in Figure 4. It remains flat until 1.5 eV/Å at its constant maximum value of −2.98 $\mu_B$ and then gradually decreases to −2.92 $\mu_B$ at 3.5 eV/Å. The same dependence is fair for the $NiI_2$ fragment (Table S1).

The analysis of spatial distribution of frontier energetic levels of the spinterface was performed to identify the contributions of the fragments in VB top and CB bottom (Figure 5). For the spinterface with ferromagnetic ordering the spatial electronic density of VB top is localized at the NiI2 fragment, while the CB bottom is localized at the CoI2 Co $d_{z^2}$ orbitals, so it can be suggested that electrons are going to be transferred to the NiI2 fragment at first. The external field shifts the original VB top state down in energy, so the modified VB top is presented by the bonding I$p_x$ orbitals of the $CoI_2$ fragment. In general, it means that electronic transfer will be more efficient in field condition than in its absence because of transmission within a $CoI_2$ fragment.

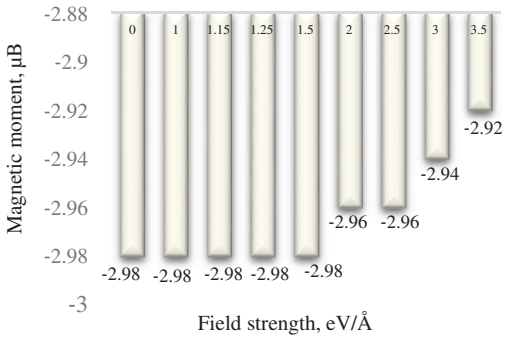


**FIGURE 4** Magnetic moments of $NiI_2$ film dependence on the electric field strength

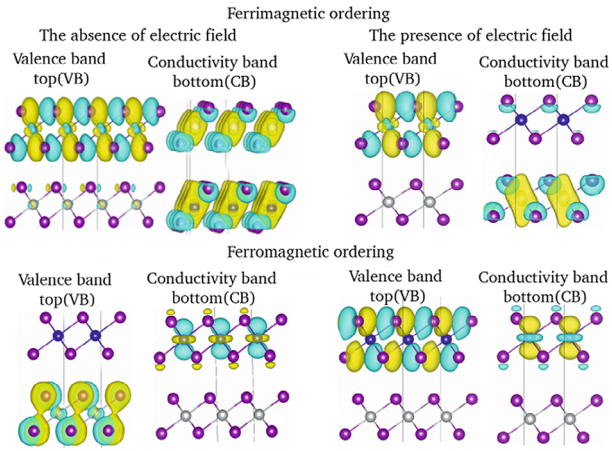


**FIGURE 5** Valence top and conductivity bottom bands of the spinterface of different spin ordering with and without external electric field. The Co and Ni ions are presented in blue and gray, respectively. The I ions are in purple. Yellow and blue areas are denoted to be negative and positive signs of wavefunction, respectively

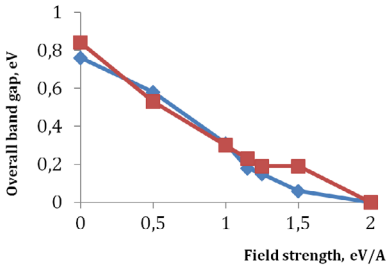


**FIGURE 6** Overall band gap dependence on the electric field strength. The red line corresponds to ferrimagnetic spin ordering, and blue line corresponds to ferromagnetic spin ordering

For the spinterface with ferrimagnetic ordering, the spatial electronic density of VB top is localized at the $CoI_2$ fragment, while CB bottom is localized at both the $CoI_2$ and $NiI_2$ fragments. The impact of the external electric field is determined through the vanishing of the CB bottom localization at $CoI_2$ fragment.It particularly defines complication at electronic transfer due to VB top and CB bottom distribution at different fragments.

To analyze the conducting properties of the interface under external electric field, a set of band structure calculations was performed (Figure 6). For both types of spin ordering, the interface demonstrates semiconducting properties and retains them up to an electric field strength of 2 eV/Å. As can be seen in Figure 4, the tendency of the band gap width decrease is characterized by linear dependence with a slight deviation at 1.5 eV/A for ferrimagnetic ordering, while ferromagnetic ordering downtrend looks quite smooth.

The band gap data are presented in Table 2. The ferromagnetic interface is a narrow band gap semiconductor with an indirect overall band gap of 0.76 eV with maximum CB at Γ point and minimum VB at Γ/M point of Brillouin zone.

The spin-resolved band gaps are equal to 1.15 and 2.89 eV for α and β spin states, respectively. The ferrimagnetic interface is a narrow band gap semiconductor with an indirect overall band gap of 0.84 eV with maximum CB at Γ point and minimum VB at Γ/M point of Brillouin zone with spin-resolved band gaps equal to 0.83 and 1.08 eV for α and β spin states, respectively.

Figure 7 illustrates a drastic decrease of the band gap width as the external electric field is applied, leading to the change of interface's electronic state nature for both ferromagnetic and ferrimagnetic states. At high external electric field, both α CB and VB cross the Fermi level at Γ, K/Γ points of Brillouin zone, and the ferromagnetic spinterface becomes a half-metallic composite in α channel at a strength of electric field of 2.0 eV/Å. At the same conditions, both β CB and α VB cross the Fermi level at Γ, K/Γ points, and ferrimagnetic spinterface becomes a zero-gap spin-polarized semiconductor. Full data of the band gap analysis for field conditions are presented in Table 2 and in Figure S4 to S12.

**TABLE 2** Overall and spin-resolved band gaps of the spinterface without field/1.15 eV/Å field

| | Ferromagnetic state | | | Ferrimagnetic state | | |
|---|---|---|---|---|---|---|
| | Overall band gap | Band gap (spin $\alpha$) | Band gap (spin $\beta$) | Overall band gap | Band gap (spin $\alpha$) | Band gap (spin $\beta$) |
| Band gap width (eV) | 0.76/0.18 | 1.15/2.39 | 2.89/0.57 | 0.84/0.23 | 0.83/0.23 | 1.08/1.48 |
| Type | Indirect/Indirect | Indirect/Indirect | Indirect/Indirect | Indirect/Indirect | Indirect/Indirect | Direct/Direct |

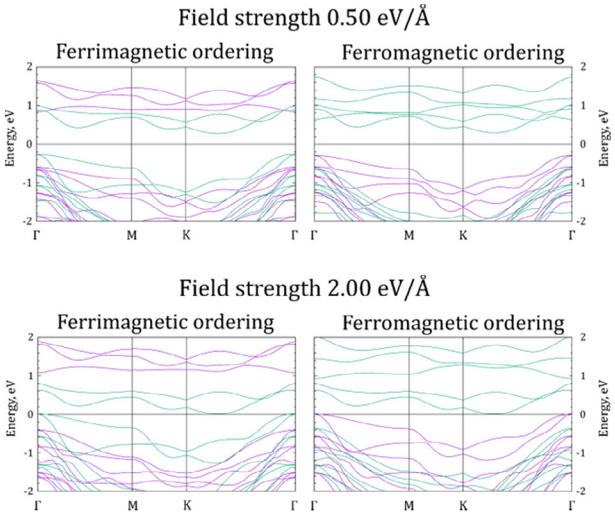


**FIGURE 7** Band structures of $CoI_2/NiI_2$ interface under applied external electric field in the range of 0.5 to 2.0 eV/Å. Green lines refer to spin α, and purple lines refer to spin β

## 4 | CONCLUSIONS

Using PBE + U electronic structure calculations, it was found that the $CoI_2/NiI_2$ heterostructure is a spin-polarized narrow band gap semiconductor. Two possible magnetic states of the interface were considered, namely, ferro- and ferrimagnetic ordering between the layers. The nature of external electric field impact was investigated using electronic structure calculations. It was found that an increase of the external electric field strength leads to the narrowing of the band gap, retaining its indirect nature. The application of the external electric field leads to the change of the electronic properties from semiconducting to half-metallic, making the $CoI_2/NiI_2$ interface a good candidate for spintronics applications.

## ACKNOWLEDGMENTS

The authors thank the Joint Supercomputer Center of RAS, Moscow; Center of Equipment for Joint Use of Siberian Federal University, Krasnoyarsk; and Information Technology Centre, Novosibirsk State University for providing access to their supercomputers. The authors also express their gratitude to language advisor E.S. Muchkina for her contribution to the manuscript. This work was supported by the government contract of the Ministry of Education and Science of the Russian Federation to Siberian Federal University (Grant No. 16.1455.2017/PCh). E.A.K. thanks the Russian Foundation for Basic Research, Government of Krasnoyarsk Territory, Krasnoyarsk Regional Fund of Science to the research project (Grant No: 18-43-243011). "Quantum chemical modeling of Bychkov-Rashba interfaces based on transition metal compounds and nanoscaled organic fragments." P.V.A. and I.M. acknowledge the National Research Foundation of the Republic of Korea for support under grant NRF-2017R1A2B4004440.

## ORCID

*Iuliia Melchakova* https://orcid.org/0000-0003-4694-2995

## REFERENCES

[1] J. Chen, Y. Shi, Y. He, T. Zhai, *FlatChem* **2019**, *17*, 100116.
[2] K. S. Novoselov, A. K. Geim, S. V. Morozov, D. Jiang, Y. Zhang, S. V. Dubonos, I. V. Grigorieva, A. A. Firsov, *Science* **2004**, *306*, 666.
[3] L. Verger, C. Xu, V. Natu, H.-M. Cheng, W. Ren, M. W. Barsoum, *Curr. Opin. Solid State Mater. Sci.* **2019**, *23*, 149.
[4] K. S. Novoselov, A. K. Geim, S. V. Morozov, D. Jiang, M. I. Katsnelson, I. V. Grigorieva, S. V. Dubonos, A. A. Firsov, *Nature* **2005**, *438*, 197.

[5] T. Li, H. Wang, D. Ma, K. Li, Z. Hu, *Mater. Res. Bull.* **2019**, *115*, 116.
[6] S. Zhang, Y. Li, T. Zhao, Q. Wang, *Sci. Rep.* **2014**, *4*, 5241.
[7] A. V. Kuklin, A. A. Kuzubov, E. A. Kovaleva, N. S. Mikhaleva, F. N. Tomilin, H. Lee, P. V. Avramov, *Nanoscale* **2017**, *9*, 621.
[8] Y. Ni, Y.-D. Guo, X.-H. Yan, H.-L. Zeng, Y. Zhang, X.-Y. Chen, X.-Y. Shen, *Phys. Lett. A* **2019**, *383*, 1636.
[9] Y. Yang, Y. Zhang, H. Ye, Z. Yu, Y. Liu, B. Su, W. Xu, *Superlattices Microstruct.* **2019**, *131*, 8.
[10] Z. I. Popov, N. S. Mikhaleva, M. A. Visotin, A. A. Kuzubov, S. Entani, H. Naramoto, S. Sakai, P. B. Sorokin, P. V. Avramov, *Phys. Chem. Chem. Phys.* **2016**, *18*, 33047.
[11] H. Shi, H. Pan, Y.-W. Zhang, B. I. Yakobson, *Phys. Rev. B* **2013**, *88*, 205305.
[12] S. Wen, H. Pan, Y. Zheng, *J. Mater. Chem. C* **2015**, *3*, 3714.
[13] H. Pan, *J. Phys. Chem. C* **2014**, *118*, 13248.
[14] J. M. Friedt, J. P. Sanchez, G. K. Shenoy, *J. Chem. Phys.* **1976**, *65*, 5093.
[15] S. Roy Chowdhury, S. Manna, S. Mishra, *Chem. Phys.* **2018**, *515*, 513.
[16] S. R. Kuindersma, J. P. Sanchez, C. Haas, *Phys. B+C* **1981**, *111*, 231.
[17] E. A. Kovaleva, I. Melchakova, N. S. Mikhaleva, F. N. Tomilin, S. G. Ovchinnikov, W. Baek, V. A. Pomogaev, P. Avramov, A. Kuzubov, *J. Phys. Chem. Solids.* **2019**, *134*, 324.
[18] J. P. Perdew, J. A. Chevary, S. H. Vosko, K. A. Jackson, M. R. Pederson, D. J. Singh, C. Fiolhais, *Phys. Rev. B* **1992**, *46*, 6671.
[19] J. P. Perdew, J. A. Chevary, S. H. Vosko, K. A. Jackson, M. R. Pederson, D. J. Singh, C. Fiolhais, *Phys. Rev. B* **1993**, *48*, 4978.
[20] I. Morrison, D. M. Bylander, L. Kleinman, *Phys. Rev. B* **1993**, *47*, 6728.
[21] M. D. Hunter, *Struct. Equ. Model. A Multidiscip. J.* **2018**, *25*, 307.
[22] V. I. Anisimov, J. Zaanen, O. K. Andersen, *Phys. Rev. B* **1991**, *44*, 943.
[23] S. L. Dudarev, G. A. Botton, S. Y. Savrasov, C. J. Humphreys, A. P. Sutton, *Phys. Rev. B* **1998**, *57*, 1505.
[24] H. J. Monkhorst, J. D. Pack, *Phys. Rev. B* **1976**, *13*, 5188.
[25] P. V. Avramov, D. G. Fedorov, P. B. Sorokin, S. Sakai, S. Entani, M. Ohtomo, Y. Matsumoto, H. Naramoto, *J. Phys. Chem. Lett.* **2012**, *3*, 2003.
[26] P. Avramov, V. Demin, M. Luo, C. H. Choi, P. B. Sorokin, B. Yakobson, L. Chernozatonskii, *J. Phys. Chem. Lett.* **2015**, *6*, 4525.
[27] P. V. Avramov, A. A. Kuzubov, S. Sakai, M. Ohtomo, S. Entani, Y. Matsumoto, H. Naramoto, N. S. Eleseeva, *J. Appl. Phys.* **2012**, *112*, 114303.

## SUPPORTING INFORMATION

Additional supporting information may be found online in the Supporting Information section at the end of this article.

**How to cite this article:** Melchakova I, Kovaleva EA, Mikhaleva NS, et al. External electric field effect on electronic properties and charge transfer in $CoI_2$/$NiI_2$ spinterface. *Int J Quantum Chem*. 2020;120:e26092. https://doi.org/10.1002/qua.26092